Insights into alpha-K toxin specificity for K+ channels revealed through mutations in noxiustoxin.

6 AUTHORS, INCLUDING:

Edward P Christian

38 PUBLICATIONS **1,573** CITATIONS

SEE PROFILE

Kathleen Giangiacomo

Temple University

23 PUBLICATIONS **1,028** CITATIONS

SEE PROFILE

Insights into α-K Toxin Specificity for K+ Channels Revealed through Mutations in Noxiustoxin[†]

Theodore J. Mullmann,[‡] Katherine T. Spence,[§] Nathan E. Schroeder,[‡] Valerie Fremont,[‡] Edward P. Christian,[§] and Kathleen M. Giangiacomo*,[‡]

*Department of Biochemistry, Temple University School of Medicine, 3420 North Broad Street,
Philadelphia, Pennsylvania 19140, and Department of Neuroscience, Astra-Zeneca Pharmaceuticals, 1800 Concord Pike,
Wilmington, Delaware 19850*

ABSTRACT: Noxiustoxin (NxTX) displays an extraordinary ability to discriminate between large conductance, calcium-activated potassium (maxi-K) channels and voltage-gated potassium (Kv1.3) channels. To identify features that contribute to this specificity, we constructed several NxTX mutants and examined their effects on whole cell current through Kv1.3 channels and on current through single maxi-K channels. Recombinant NxTX and the site-specific mutants (P10S, S14W, A25R, A25Δ) all inhibited Kv1.3 channels with K_d values of 6, 30, 0.6, 112, and 166 nM, respectively. In contrast, these same NxTX mutants had no effect on maxi-K channel activity with estimated K_d values exceeding 1 mM. To examine the role of the α-carbon backbone in binding specificity, we constructed four NxTX chimeras, which altered the backbone length and the α/β turn. For each of these chimeras, six amino acids comprising the α/β turn in iberiotoxin (IbTX) replaced the corresponding seven amino acids in NxTX (NxTX-YGSSAGA$_{21−27}$-FGVDRG$_{21−26}$). The chimeras differed in length of N- and C-terminal residues and in critical contact residues. In contrast to NxTX and its site-directed mutants, all of these chimeras inhibited single maxi-K channels. Under low ionic strength conditions, K_d values ranged from 0.4 to 6 μM, association rate constant values from 3×10^7 to 3×10^8 M^{-1} s^{-1}, and time constants for block from 5 to 20 ms. The rapid blocked times suggest that key microscopic interactions at the toxin−maxi-K channel interface may be absent. Under physiologic external ionic strength conditions, these chimera inhibited Kv1.3 channels with K_d values from 30 to 10 000 nM. These results suggest that the extraordinary specificity of NxTX for Kv1.3 over maxi-K channels is controlled, in part, by the toxin α-carbon backbone. These differences in the α-carbon backbone are likely to reflect fundamental structural differences in the external vestibules of these two channels.

The α-K channel toxin (α-KTx)[1] peptides inhibit the flow of K+ ions through the K+ channel pore by simply binding to and occluding the extra cellular pore. This simple, bimolecular plugging mechanism is based on detailed kinetic studies of toxin block of single large-conductance, calcium-activated potassium (maxi-K) channels (*1, 2*) and of macroscopic current through a voltage-gated potassium (Kv) channel (*3*). The location of the α-KTx binding site to the external vestibule has revealed amino acids that form the potassium channel pore (*4, 5*), and it has yielded a low-resolution image of the maxi-K and Kv (*6−11*) channel vestibules. Thus, the α-KTx peptides provide invaluable

molecular insight into protein structures that underlie gating and permeation in the K channel pore.

The α-KTx peptides can be grouped into different subfamilies (α-KTx 1.x, α-KTx 2.x, and α-KTx 3.x) on the basis of differences in their amino acid sequences (*12, 13*). These α-KTx subfamilies display an extraordinary ability to distinguish between the large family of voltage-gated potassium (Kv) channels and the large-conductance calcium-activated potassium (maxi-K) channel (*12*). The peptides from the α-KTx 1.x subfamily display high-affinity interactions for the maxi-K channel. However, only two of these toxins, iberiotoxin (IbTX or α-KTx 1.3) and limbatus toxin (LbTX or α-KTx 1.4), appear to be highly selective for the maxi-K channel (*14, 15*). Other toxins from this subfamily show high-affinity interactions with some Kv channels. For instance, charybdotoxin (ChTX or α-KTx 1.1) and LQ2 (α-KTx 1.2) inhibit the Kv1.3 (*16*) and Shaker Kv (*17*) channels with high affinity, respectively. Indeed, with the exception of IbTX, many of the α-KTx peptides from different subfamilies interact with the Kv1.3 channel with high affinity. In stark contrast, the α-KTx 2.x and α-KTx 3.x subfamily of toxins that block Kv channels with high affinity do not block the maxi-K channel with high affinity (*12*). Thus, the Kv1.3 channel is rather promiscuous in its

* Corresponding author. E-mail: giang@unix.temple.edu. Phone: 215-707-8170. Fax: 215-707-7536.
[‡] Temple University School of Medicine.
[§] Astra-Zeneca Pharmaceuticals.

[1] Abbreviations: α-KTx, potassium channel toxin; α-KTx 1.1, charybdotoxin; α-KTx 1.2, LQ2; α-KTx 1.3, iberiotoxin; α-KTx 2.1, noxiustoxin; α-KTx 3.2, agitoxin 2; AgTX2, agitoxin 2; ChTX, charybdotoxin; IbTX, iberiotoxin; NxTX, noxiustoxin; K_d, equilibrium dissociation constant; k_{off}, dissociation rate constant; k_{on}, second-order association rate constant; Kv channel, voltage-gated potassium channel; maxi-K channel, large-conductance calcium-activated potassium channel; P_o, single-channel open probability; T_{block}, time constant for toxin block.

interactions with α-KTx peptides while the maxi-K channel exhibits extraordinary specificity among the α-KTx subfamilies. These differences in specificity likely point to fundamental differences in the structure of the maxi-K and Kv channel vestibules.

The three-dimensional, solution NMR structures of the α-KTx peptides provide insight into the determinants for specificity (*12*). All of these peptides show a classic motif with three antiparallel β-strands forming a β-sheet face on one side of the molecule and a helix on the other. This rigid structure is maintained by the presence of three disulfide bonds that are conserved among the α-KTx peptides (*12*). Thus, all of the α-KTx peptides share a similar 3D structure. However, among the α-KTx subfamilies, there are differences in the α-carbon backbone that may contribute to differences in binding specificity. The most striking differences occur between the α-KTx 2.x and α-KTx 1.x subfamilies; see Figure 1. The α-KTx 2.x subfamily contains two extra amino acids that extend the N- and C-termini, each by one residue relative to the α-KTx 1.x toxins (*12*). In addition, the α/β turns in α-KTx 1.x and α-KTx 2.x show structural differences (*12*). The structural differences between these two subfamilies may contribute to their specificity for maxi-K versus Kv channels.

Insight into the determinants for this specificity also comes from knowledge of toxin residues that form an interaction surface with the maxi-K channel. Identification of toxin residues critical for a high-affinity interaction with the maxi-K channel comes from site-directed mutagenesis studies with ChTX (*11*). This work showed that eight residues, protruding from the ChTX β-sheet face, are critical for a high-affinity interaction with the maxi-K channel (Figure 1). Moreover, two of these residues, R25 and W14, are unique to the α-KTx 1.x subfamily (*12*). However, these maxi-K channel contact residues are not well conserved among the α-KTx 2.x and α-KTx 3.x subfamilies. Thus, the absence of this repertoire of critical contact residues among the α-KTx 2.x and α-KTx 3.x subfamilies may contribute to their discrimination against the maxi-K channel.

Noxiustoxin (NxTX or α-KTx 2.1) is an exquisite discriminator of maxi-K versus Kv1.3 channels. In this work, we show that the difference in NxTX binding free energy for the maxi-K and Kv channels exceeds 7 kcal/mol. To test whether this specificity derives from the absence of critical contact residues or from differences in the α-carbon backbone, we constructed various site-specific and chimeric NxTX mutants and examined their functional interaction with Kv1.3 and maxi-K channels. Remarkably, we found that altering the toxin α-carbon backbone had profound effects on toxin binding specificity for the maxi-K and Kv channels.

MATERIALS AND METHODS

Materials. Sarcolemmal membranes from bovine aortic smooth muscle were purified as described (*18*). The plasmid construct pG9-M was a generous gift from Dr. Maria Garcia (Merck Research Laboratories).

Polystyrene cuvettes for bilayer experiments contained either a 100 or 150 μm aperture and were purchased from Warner Instruments, Inc. (Hamden, CT). 1-Palmitoyl-2-oleoylphosphatidylethanolamine (POPE) and 1-palmitoyl-2-oleoylphosphatidylcholine (POPC) were from Avanti Polar Lipids, Inc. (Birmingham, AL). Decane from Fisher Scientific, Inc. (Springfield, NJ), was 99.9% mole purity. All other reagents were of the highest purity commercially available.

Construction of the NxTX Plasmid and Mutants. The plasmid pG9-NxTX, encoding six histidine residues between the T7 gene 9 fusion protein and the factor Xa cleavage site, and the wild-type NxTX sequence were constructed as described (*19*). NxTX mutations were generated using a two-step polymerase chain reaction point mutagenesis strategy. Plasmids containing the NxTX gene and site-directed mutants were propagated using the *Escherichia coli* strain DH5α. The identity of all DNA constructs was verified using dideoxy sequencing (*20*).

Expression and Purification of Recombinant Noxiustoxin Mutants. The *E. coli* strain BL21(DE3) harboring the pG9-NxTX plasmids was cultured and induced with isopropyl 1-thio-β-galactopyranoside (IPTG), and the T7 gene 9 toxin fusion protein was purified by DEAE ion-exchange chromatography as described (*19*) with the following modifications. After folding, the fusion protein was cleaved from the toxin with TPCK-treated trypsin as described (*21*). This reaction was inhibited with L-1-chloro-3-(4-tosylamido)-7-amino-2-heptanone hydrochloride (TLCK) and immediately loaded onto a 300 mL SP-Sephadex column equilibrated at pH 9.0 with 20 mM sodium borate and then eluted with a linear gradient of NaCl (0 to 0.75 M in 0.5 h) at a flow rate of 5 mL/min. Final purification of the peptides was achieved by reverse-phase HPLC as described (*19*). The purity of each peptide was >99% as judged by HPLC chromatography and mass spectrometric analysis. The identity of each peptide was confirmed by MALDI-MS mass spectrometric analysis (Protein Chemistry Laboratory, University of Pennsylvania). The predicted and measured masses for each peptide, respectively, were NxTX (4202, 4202), P10S (4192, 4197), S14W (4301, 4319), A25R (4287, 4288), A25Δ (4131, 4131), NxTX–IbTX I (4241, 4241), NxTX–IbTX II (4124, 4129), NxTX–IbTX III (4247, 4350), and NxTX–IbTX IV (4283, 4382). With the exception of NxTX–IbTX III and NxTX–IbTX IV, the measured masses were well within experimental error of the MALDI-MS instrumentation (Dr. William Moore, Protein Chemistry Laboratory, University of Pennsylvania, personal communication). The masses of these two mutants were further confirmed by amino acid analysis. Amino acid analyses performed on rNxTX, NxTX-S14W, NxTX–IbTX I, NxTX–IbTX II, NxTX–IbTX III, and NxTX–IbTX IV (Commonwealth Biotechnologies, Inc.) were in excellent agreement with the predicted mass of each peptide. Correct folding and disulfide bond formation for NxTX–IbTX I and NxTX–IbTX II is inferred from their solution NMR structures (*37*) and from the fact that all NxTX mutants elute with similar (∼13%) organic solvent by HPLC. The extinction coefficient for wild type, 12.82 cm^{-1} (mg/mL)$^{-1}$ at 214 nm, was used for all mutants except NxTX-S14W, 13.94 cm^{-1} (mg/mL)$^{-1}$ at 214 nm. The NxTX extinction coefficient was based on the extinction coefficient for margatoxin (MgTX or α-KTx 2.2), a peptide that displays 82% sequence identity with NxTX (*19*) and a nearly identical 3D structure (*22*). The extinction coefficient for NxTX-S14W was calculated by determining the amino acid composition of 1 nmol of toxin. Protein content was then correlated with absorbance monitored at 214 nm.

Recordings of Maxi-K Channels in Planar Lipid Bilayers. Planar lipid bilayers were formed, and maxi-K channels from membranes were fused with the artificial bilayer as described previously (*1*). The orientation of the maxi-K channel was determined by the voltage and calcium dependence of channel gating as described (*1*). The lipid composition of the planar lipid bilayer consisted of a POPE:POPC in a 7:3 molar ratio. The exact composition of the solutions on either side of the bilayer is as described in the figure legends.

Currents through single maxi-K channels were detected and amplified using a Dagan 3900A integrating patch clamp amplifier as described (*1*). Currents were recorded onto a videocassette tape and were digitally encoded on-line as described (*23*).

The single-channel currents were refiltered off-line as described (*23*), and opening and closing events were detected using a threshold detection algorithm in TAC (Bruxton Corp.). Toxin blocked times for NxTX−IbTX II were distinguished from closed times as described (*1*) except that control periods were 5 min in duration and the cutoff for block, determined from control, was typically 2−3 ms.

Amplitude Distribution Analysis of Toxin-Blocked Events. "Fast" toxin-blocked events, not well separated from closed times due to gating, were analyzed by an amplitude distribution method (*24, 25*). Digitized records representing 5 min of single-channel recording were refiltered with a digital Gaussian filter in TAC (Bruxton Corp.) so that the single pole dead time exceeded the time constant for toxin block estimated from closed time distributions. Amplitude histograms were collected in TAC before (447 Hz) and after refiltering (≤20 Hz) and exported as Igor Text files for further analysis in Igor Pro (Wavemetrics Inc.). Before being fitted to a β distribution, the current amplitudes of the experimental histograms were normalized to the unblocked open channel current level such that closed and open channel current values correspond to 0 and 1, respectively. The amplitude of the unblocked current was obtained from amplitude histograms of records with an effective filtering of 447 Hz, where the closed and open current levels are well resolved. The normalized amplitude distributions were then fit to a β distribution of the form shown in the equation (*24, 25*):

$$f(i) = \frac{i^{(\alpha T - 1)}(1 - i)^{(\beta T - 1)}}{C} \qquad (1)$$

where i is the normalized single-channel current amplitude, C is a normalization factor, and T is the first-order filter time constant. α and β describe the toxin dissociation rate constant (k_{off}) and the pseudo-first-order association rate constant (k_{on}-[toxin]), respectively. The equilibrium dissociation constant (K_d) values were calculated from the ratio of the binding rate constant values, where $K_d = k_{off}/k_{on}$.

Recordings of the Macroscopic Kv1.3 Current. Ionic currents were recorded from Jurkat E6-1 cells at room temperature (20−22 °C) using the conventional whole cell patch configuration (*26*). Jurkat cells were cultured as previously described (*27*). Recordings were carried out in a bath solution consisting of (mM) 160 NaCl, 5 KCl, 2 CaCl₂, 2 MgCl₂, 6 glucose, and 5 HEPES, pH 7.4, 325 mOsm. The intracellular pipet solution contained (mM) 140 potassium gluconate, 1 CaCl₂, 2 MgCl₂, 5 HEPES, and 10 EGTA, pH

Table 1: Amino Acid Sequences of NxTX, IbTX, and the NxTX−IbTX Chimeras[a]

NxTX	TIINVKCTSPKQCSKPCKELYGSSAG<u>A</u>KCMNGKCKCYNN
NxTX-IbTX I	TIINVKCTSPKQCSKPCKEL**FGV-DRG**KCMNGKCKCYNN
NxTX-IbTX II	-IINVKCTSPKQC**W**KPCKEL**FGV-DRG**KCMNGKCKCYN-
NxTX-IbTX III	TIINVKCTSPKQC**W**KPCKEL**FGV-DRG**KCMNGKC**R**CYN-
NxTX-IbTX IV	**TFD**NVKCTSPKQC**W**KPCKEL**FGV-DRG**KCMNGKC**R**CYN-
IbTX	**ZFTDVDCSVSKECWSVCKDLFGV-DRGKCMGKKCRCYQ**
	* * * * ** * *

[a] The asterisk indicates residues critical for binding to the maxi-K channel.

7.2, 315 mOsm. Pipets were fabricated from thin-wall borosilicate glass (1.5 mm o.d., 1.12 mm i.d.) and fire polished to a DC resistance of 2−8 MΩ. Membrane currents were amplified with either an Axopatch 1B, 200A, or 200B amplifier (Axon Instruments, Foster City, CA), low pass filtered at 1 kHz with an eight-pole Bessel filter, and then digitized at 3−5 kHz as computer files with a Digidata 1200 interface (Axon Instruments, Foster City, CA). Voltage clamp protocols were implemented, and data acquisition was performed with pClamp 6.0 software (Axon Instruments, Foster City, CA). A P4-P6 leak subtraction protocol was applied on-line to remove voltage-independent current components. Origin software (Microcal, Northampton, MA) was used to iteratively fit concentration response data to a Hill function (see Figure 2 legend). To measure current, cells were depolarized at 30 s intervals to +20 mV for 200 ms from a holding potential of −80 mV. The outward current elicited with this protocol in these Jurkat cells had the biophysical properties and sensitivity to α-KTx's that have been well established as a signature of Kv1.3 in prior studies (*27*).

RESULTS

Residues near the NxTX β-Sheet Face Form Its Interaction Surface with the Kv1.3 Channel. NxTX and peptides from the α-KTx 1.x subfamily differ in three residues that are critical for a high-affinity interaction with the maxi-K channel, S10, W14, and R25; see Table 1 and Figure 1. To understand how these residues influence NxTX block of Kv1.3 channels, we examined the effects of rNxTX and the site-directed mutants P10S, S14W, A25R, and A25Δ on macroscopic currents through Kv1.3 channels; see Figure 2 and Table 2. Figure 2A shows the effects of 0, 10, and 1000 nM rNxTX (top) and 0, 1, and 30 nM rNxTX-S14W (middle) on outward K⁺ current elicited from application of a 200 ms depolarizing step to +20 mV from a −80 mV holding potential. Both of the recombinant NxTX peptides reversibly block current through Kv1.3 channels with nanomolar potency. Interestingly, the S14W mutant peptide appears to inhibit Kv1.3 current at ∼10-fold lower concentration than wild type. A quantitative description of these effects is shown in Figure 2B as plots of fractional current remaining vs toxin concentration for rNxTX and S14W. The solid lines represent best fits of the data to simple, single-site Langmuir binding isotherms with K_d values of 6 and 0.6 for NxTX and S14W, respectively. The K_d values for NxTX and the site-directed mutants P10S, S14W, A25R, and A25Δ are shown in Table 2. Each of these NxTX mutations causes significant changes in toxin binding free energy ranging from 0.9 to 1.9 kcal/mol. This result suggests that these residues contribute to
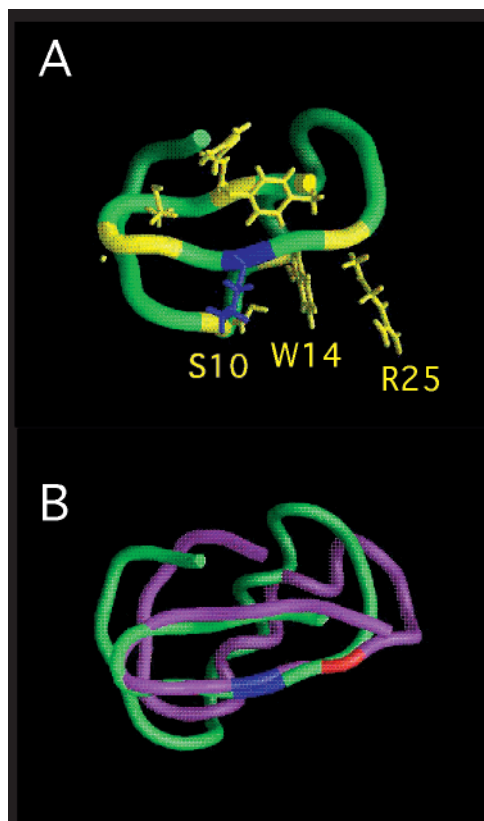
FIGURE 1: α-KTx subfamilies differ in their α-carbon backbone and in residues at the toxin−channel interface. (A) shows the α-carbon backbone structure for a high-affinity maxi-K channel inhibitor (α-KTx 1.3 or IbTX) (*39*) with the side chain bonds for the eight conserved critical contact residues shown in blue (K27) or yellow (S10, W14, R25, M29, G30, R34, Y36). Lys27 interacts with a K$^+$ binding site in the maxi-K channel pore (*23*, *32*). S10, W14, and R25 were incorporated into NxTX in this work and are the α-KTx 1.x residues critical for a high-affinity interaction with the maxi-K channel. (B) shows the superimposed α-carbon backbone structures for α-KTx 1.3 (IbTX) in green and for α-KTx 2.1 or NxTX (*28*) in magenta. The structures were aligned by superposition of conserved residues in the second and third antiparallel β-strands. The strictly conserved Lys27 is colored in blue.

the NxTX−Kv1.3 interaction surface. The location of these residues, in or near the β-sheet face and α/β turn, suggests that these regions of the NxTX structure (*28*) interact with the Kv1.3 outer vestibule; see Figure 1.

In contrast, these same NxTX mutants had no effect on current through single maxi-K channels at $10-20$ μM concentrations, under physiological external ionic strength conditions (Table 3). Estimated K_d values for these NxTX mutants exceed 1 mM. This calculation was based on the finding that stability plots of single-channel open probability (P_o) in the absence and presence of toxin differed by less than 2%. We also examined the effects of these mutants when KCl was 150 mM inside and outside and observed no effect (not shown). Thus, the inclusion of these critical residues into NxTX does not promote a measurable interaction with the maxi-K channel. Together, these results suggest that maxi-K and Kv1.3 channels display different determinants for binding specificity. Moreover, they suggest that the absence of critical toxin residues is not the only factor limiting a high-affinity interaction between NxTX and the maxi-K channel vestibule.
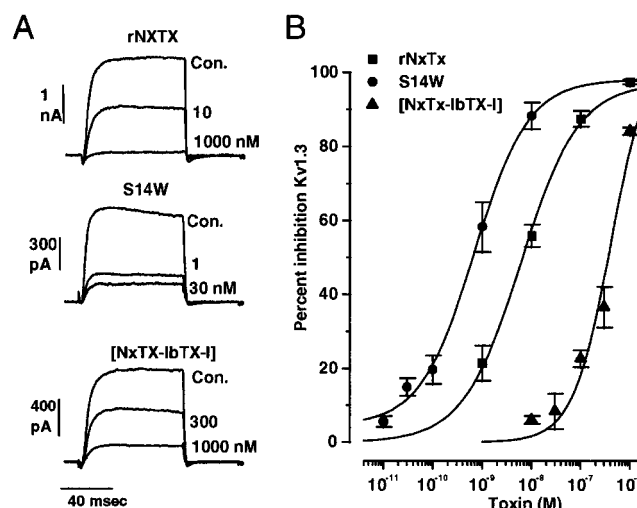

FIGURE 2: Effect of NxTX mutants on macroscopic current through Kv1.3 channels. (A) Whole cell current recording from Jurkat cells in the absence and presence of the indicated concentrations of rNxTX, NxTX-S14W, and NxTX−IbTX I. (B) Dose-dependent inhibition curves for block of macroscopic Kv1.3 current by rNxTX, NxTX-S14W, and NxTX−IbTX I. Macroscopic current in the presence of toxin, normalized to current measured in the absence of toxin, represents the average of three to seven separate determinations, and error bars represent the standard error of the mean. The line represents the best fit of the data to a Hill equation of the form $I/I_{max}(100) = 100/[1 + (IC_{50}/x)^{n_H}]$, where I and I_{max} are the current amplitudes measured in the presence and absence of a given toxin concentration (x), IC_{50} is the concentration producing 50% current block, and n_H is the Hill coefficient, respectively. K_d values obtained from the fit were 0.6, 6, and 355 nM for NxTX-S14W, NxTX, and NxTX−IbTX I, respectively.

Table 2: Equilibrium Dissociation Constant Values for Toxin Block of Whole Cell Current through Kv1.3 Channels

rNxTX mutant	K_d (nM)[a]	Hill slope[a]
wild type	6.8	0.72
P10S	30	0.75
S14W	0.61	0.72
A25R	112	0.83
A25Δ	166	0.83
NxTX−IbTX I	355	1.12
NxTX−IbTX II	≥10000	
NxTX−IbTX III	19	1.13
NxTX−IbTX IV	356	0.93

[a] K_d values and Hill slopes were obtained from Hill fits of concentration−response data of toxin concentration vs percent inhibition of control Kv1.3 current in Jurkat cells; see Figure 2.

Changes in the NxTX α-Carbon Backbone Promote a Binding Interaction with the Maxi-K Channel Outer Vestibule. NxTX is a member of the α-KTx 2.x subfamily of peptide toxins that show notable differences in their α-carbon backbone when compared to the α-KTx 1.x subfamily (Figure 1) (*12*). To test whether these differences in the α-carbon backbone prevent NxTX from interacting with the maxi-K channel, we generated four NxTX chimeric mutants that were altered in the α-carbon backbone; see Table 1. For each of these chimera a stretch of seven amino acids in NxTX, YGSSAGA$_{21-27}$, was replaced with six structurally equivalent amino acids in α-KTx 1.3 (IbTX), FGVDRG$_{21-26}$. This mutation decreases the length of the α-carbon backbone at the N-terminus, and it replaces residues in the α/β turn of NxTX (α-KTx 2.1) with those of IbTX (α-KTx 1.3). NxTX−IbTX I contains this mutation alone. All of the other chimeras

Table 3: Toxin Blocking Kinetics from Single Maxi-K Channels with High External Potassium and Low Internal Potassium[a]

rNxTX mutant	V_m (mV)	$K_d P_o$[b] (μM)	K_d kinetics[c] (μM)	k_{on}[d] ($\times 10^6$ M^{-1} s^{-1})	T_{block}[d] (ms)	$K_d \beta$[c] (μM)	k_{on}[e] ($\times 10^6$ M^{-1} s^{-1})	T_{block}[e] (ms)
wild type[f]	0, +30	$\geq$1000						
P10S[f]	0, +30	$\geq$1000						
S14W[f]	0, +30	$\geq$1000						
A25R[f]	0, +30	$\geq$2000						
A25Δ[f]	0, +30	$\geq$1000						
NxTX−IbTX I[g]	0	$\geq$200						
NxTX−IbTX II	0	20 $\pm$ 5	31 $\pm$ 8	2 $\pm$ 0.6	19 $\pm$ 2	17 $\pm$ 5	2 $\pm$ 1	20 $\pm$ 3.5
	+30	42 $\pm$ 16	88 $\pm$ 10	1.2 $\pm$ 0.2	10 $\pm$ 0.5	50 $\pm$ 18	2 $\pm$ 1	15 $\pm$ 5
NxTX−IbTX III[h]	0	$\geq$13						
	+30					11 $\pm$ 4	3.5 $\pm$ 1	38 $\pm$ 24
NxTX−IbTX IV[i]	0	$\geq$70						
	+30							

[a] Conditions were as described in Figure 3 with 150 mM KCl outside and 10 mM KCl inside. [b] K_d values were obtained from fits to P_o versus toxin concentration. [c] K_d values were calculated from $K_d = k_{off}/k_{on}$, where $k_{off} = 1/T_{block}$. [d] k_{on} and T_{block} values were obtained from blocked and unblocked distributions; see Materials and Methods. [e] k_{on} and T_{block} values were obtained from amplitude distribution analysis; see Materials and Methods. [f] 10 or 20 μM applied toxins caused no detectable decrease in P_o. Lower limits for K_d values were estimated assuming single-site binding and a 0.02 change in P_o as the limit of detection. [g] In two experiments, 10 μM NxTX−IbTX I produced a significant and reproducible 0.06 decrease in P_o. [h] In two experiments, 20 and 12 μM NxTX−IbTX III caused decreases in P_o of 0.46 and 0.68, respectively, with a membrane potential of 0 mV. [i] In two experiments, 5 and 80 μM NxTX−IbTX IV caused decreases in P_o of 0.12 and 0.3, respectively, with a membrane potential of 0 mV.

Table 4: Toxin Blocking Kinetics from Single Maxi-K Channels with Low External Potassium and High Internal Potassium[a]

rNxTX mutant	V_m (mV)	K_d[b] kinetics (μM)	k_{on}[c] ($\times 10^6$ M^{-1} s^{-1})	T_{block}[c] (ms)	K_d[b] β (μM)	k_{on}[d] ($\times 10^6$ M^{-1} s^{-1})	T_{block}[d] (ms)
IbTX[e]	+30	0.0002 $\pm$ 0.0001	13 $\pm$ 6	456000 $\pm$ 63000			
NxTX[f]	0	$\geq$50					
NxTX−IbTX I	0				6.5 $\pm$ 3	36 $\pm$ 8	5 $\pm$ 1
	+30				15 $\pm$ 5	20 $\pm$ 2	3.6 $\pm$ 0.9
NxTX−IbTX II	0	0.7 $\pm$ 0.5	190 $\pm$ 100	15 $\pm$ 5	0.4 $\pm$ 0.2	180 $\pm$ 90	18 $\pm$ 0.4
	+30	1.7 $\pm$ 0.7	110 $\pm$ 21	6 $\pm$ 2	1.0 $\pm$ 0.4	130 $\pm$ 12	10 $\pm$ 2.5
NxTX−IbTX III	−20				0.17 $\pm$ 0.05	410 $\pm$ 150	20 $\pm$ 2
	0				0.43 $\pm$ 0.2	350 $\pm$ 110	13 $\pm$ 2
	+30				1.3 $\pm$ 0.6	160 $\pm$ 40	8 $\pm$ 2
NxTX−IbTX IV	−20				0.8 $\pm$ 0.1	93 $\pm$ 8	13 $\pm$ 2
	0				1.53 $\pm$ 0.04	76 $\pm$ 0.3	8.8 $\pm$ 0.2
	+30				4.7 $\pm$ 0.35	46 $\pm$ 1	4.7 $\pm$ 0.09

[a] Conditions were as described in Figure 4 with 30 mM KCl outside and 150 mM KCl inside. [b] K_d values were calculated from $K_d = k_{off}/k_{on}$, where $k_{off} = 1/T_{block}$. [c] k_{on} and T_{block} values were obtained from analysis of blocked and unblocked distributions; see Materials and Methods. [d] k_{on} and T_{block} values were obtained from amplitude distribution analysis; see Materials and Methods. [e] K_d, k_{on}, and T_{block} values for IbTX were determined with 25 mM KCl on the outside and 150 mM inside from previously published work (1). [f] 1 μM NxTX caused no detectable decrease in P_o. Lower limits for the K_d value were estimated assuming single-site binding and a 0.02 change in P_o as the limit of detection.

include the critical contact residues W14 and deletion of the C-terminal Asn residue, NxTX−IbTX III. In addition to these mutations, NxTX−IbTX II contains an additional deletion at the N-terminus, and NxTX−IbTX IV contains the mutations I2F/I3D. To include all of the critical maxi-K channel contact residues, NxTX−IbTX III and NxTX−IbTX IV additionally contain the conservative K34R mutation.

To test whether these chimeric mutants interacted with maxi-K channels, we examined their effects on current through single maxi-K channels in planar lipid bilayers with high, 150 mM external potassium. In striking contrast to NxTX, all of these chimera showed a measurable effect on single-channel open probability (P_o) at micromolar concentrations with NxTX−IbTX II and NxTX−IbTX III being the most potent; see Tables 3 and 4. Figure 3 shows the effects of NxTX−IbTX II on inward current through single maxi-K channels incorporated into planar lipid bilayers. Figure 3A shows that under physiological external ionic strength conditions micromolar concentrations of NxTX−IbTX II cause the appearance of short silent periods, ~10 ms in duration, and the frequency of these durations increases with NxTX−IbTX II concentration. This is in striking

contrast to rNxTX and its site-directed mutants where micromolar concentrations had no effect on channel activity. Figure 3B shows that, at NxTX−IbTX II concentrations where the maxi-K channel is >90% inhibited, the closed time distribution contains a 10 ms component that is distinct from the closed time distribution obtained in control. Figure 3C shows that the dose-dependent changes in P_o caused by NxTX−IbTX II are well described by a single-site Langmuir binding isotherm with a K_d value of 20 μM. This K_d value is nearly 2 orders of magnitude tighter than the value we estimate for rNxTX under identical experimental conditions. Thus, by changing the rNxTX α-carbon backbone, we have generated a mutant which blocks current through the maxi-K channel.

Low External Ionic Strength Promotes a High-Affinity Interaction between the NxTX−IbTX Mutants and the Maxi-K Channel. The NxTX−IbTX chimeric mutants are highly basic, exhibiting net charges of either +6 (chimera I, II, and III) or +5 (chimera IV). Previous studies with ChTX (29) and IbTX (23) have shown that basic toxin residues interact with the maxi-K channel vestibule to promote high rates of association. Moreover, these electrostatic interactions are
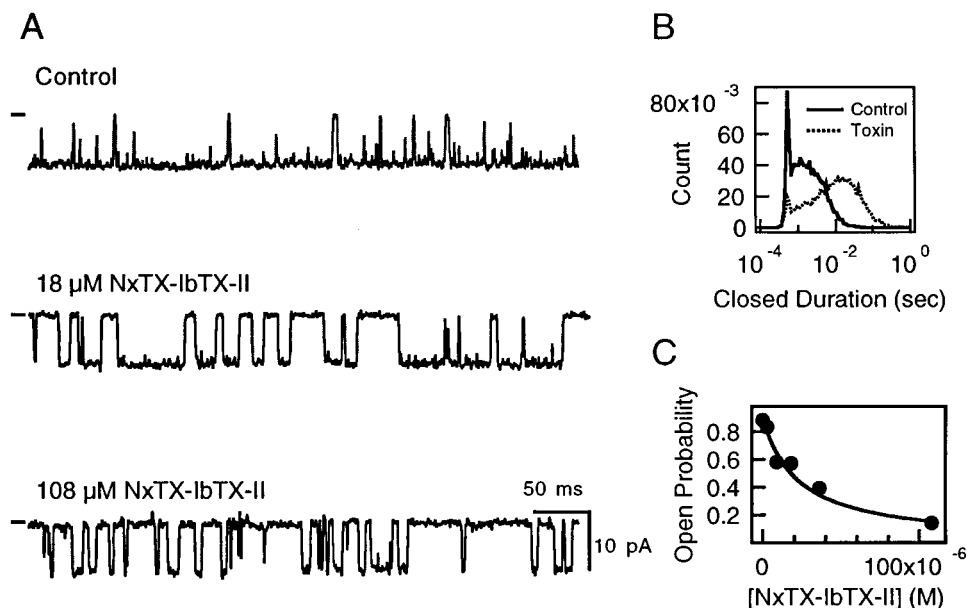
FIGURE 3: Effect of NxTX−IbTX II on single maxi-K channels when external ionic strength is high. (A) Recordings of inward single-channel current in the absence and presence of 18 and 108 μM NxTX−IbTX II. The lines to the left indicate the zero current level. Horizontal and vertical scale bars represent 50 ms and 10 pA, respectively. Records were filtered at 447 Hz and acquired at 100 μs/point. (B) Closed time distributions obtained from 5 min of recording in the absence (solid line) and presence of 108 μM NxTX−IbTX II (dotted line) are plotted as the number of events of a particular duration against their durations. The distributions were scaled to contain the same number of events. (C) Single-channel open probability (P_o) is plotted as a function of NxTX−IbTX II concentration. The solid line represents the best fit of the data to a single-site Langmuir isotherm of the form $P_o = P_o(max)/[1 + (K_d/[Toxin])]$ with a K_d value of 24 μM, where $P_o(max)$ and P_o describe values measured in the absence and presence of given toxin concentrations, respectively. Conditions were (outside) 150 mM KCl, 5 μM CaCl$_2$, (inside) 10 mM KCl, 605 μM CaCl$_2$, and (on both sides) 10 mM HEPES, pH 7.2, 3.7 mM KOH. The membrane potential was 0 mV.
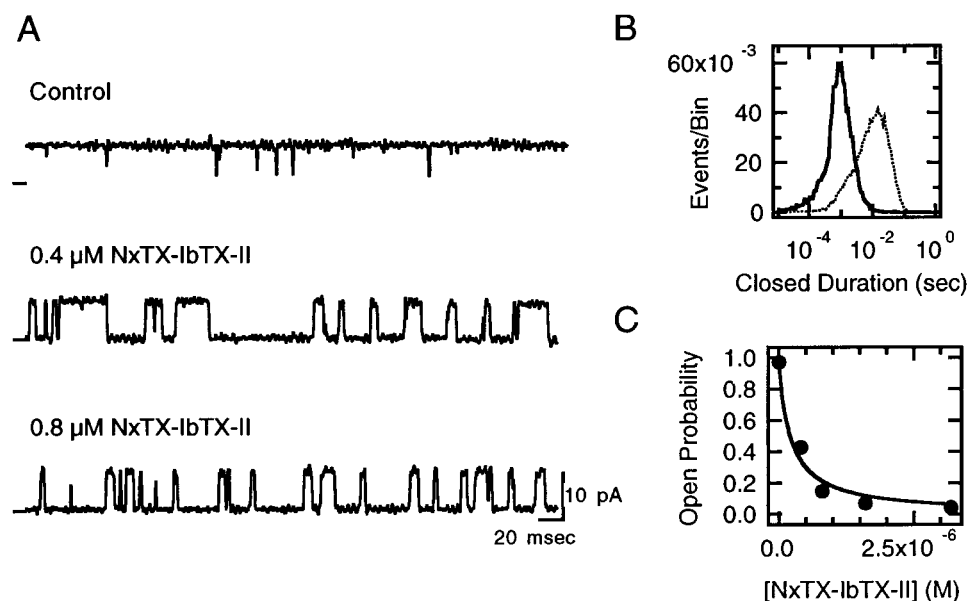

FIGURE 4: Effect of NxTX−IbTX II on single maxi-K channels when external ionic strength is low. (A) Recordings of outward single maxi-K channel current is shown in the absence and presence of 0.4 and 0.8 μM NxTX−IbTX II. The lines to the left indicate the zero current level. Horizontal and vertical scale bars represent 20 ms and 10 pA, respectively. Records were filtered at 447 Hz and acquired at 100 μs/point. (B) Closed time distributions obtained from 5 min of recording in the absence (solid line) and presence of 0.8 μM NxTX−IbTX II (dotted line) are plotted as the number of events of a particular duration against their durations. The distributions were scaled to contain the same number of events. (C) Plots P_o versus concentration of NxTX−IbTX II. The solid line represents the best fit of the data to a single-site Langmuir isotherm as described in Figure 3 with a K_d value of 222 nM. Conditions were (outside) 30 mM KCl, 5 μM CaCl$_2$, (inside) 150 mM KCl, 605 μM CaCl$_2$, and (on both sides) 10 mM HEPES, pH 7.2, 3.7 mM KOH. The membrane potential was 0 mV.

attenuated with increasing external ionic strength (*1*, *23*, *30*). Thus, electrostatic interactions observed at low ionic strength promote high-affinity toxin−channel interactions.

To test this, we examined the effects of NxTX−IbTX II on current through single maxi-K channels when external

ionic strength was low (Figure 4). Part A of Figure 4 shows that 400 nM NxTX−IbTX II cause a marked decrease in P_o relative to control (0.97 vs 0.42) that results from the appearance of brief, ~10 ms, silent periods. As expected, the frequency of these silent periods increases when the
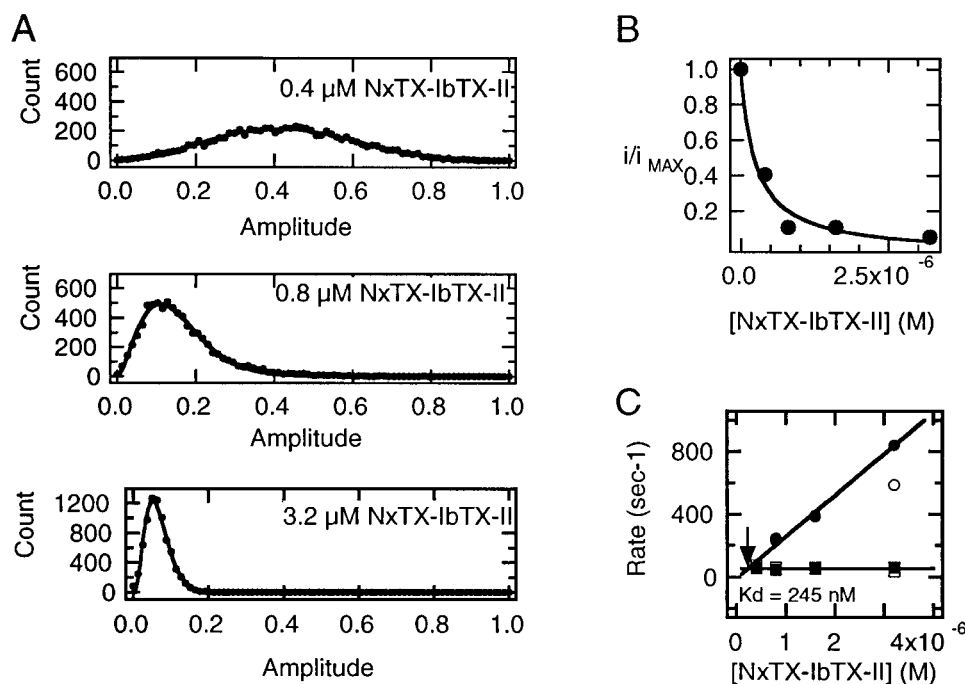
FIGURE 5: Amplitude distribution analyses of single maxi-K channel current yield NxTX−IbTX II blocking rates and K_d values. (A) plots amplitude histograms from single maxi-K channel records refiltered at 5 Hz (filled circles) in the presence of NxTX−IbTX II. The solid line represents the best of the data to a β distribution of the form $f(i) = i^{(\alpha T-1)}(1 - i)^{(\beta T-1)}/C$, where i is the normalized single-channel current amplitude, C is a normalization factor, and T is the first-order filter time constant. α and β describe the toxin dissociation rate constant (k_{off}) and the pseudo-first-order association rate constant (k_{on}[toxin]), respectively. (B) plots the normalized single-channel current amplitude as a function of NxTX−IbTX II concentration. Normalized current amplitudes (i/i_{max}) were obtained from the mode of the amplitude distributions shown in (A). The solid line represents the best fit of the data to a single-site Langmuir isotherm of the form i/i_{max} = 1/[1 + (K_d/[toxin])] with a K_d value of 245 nM. (C) plots the association (filled circles) and dissociation (filled squares) rates obtained from fits shown in (A) versus NxTX−IbTX II concentration. Association (open circles) and dissociation (open squares) rates obtained from dwell-time analysis, as described in Materials and Methods, are shown for comparison. The lines represent the best fit to a straight line. Conditions were as in Figure 4.

NxTX−IbTX II concentration is increased to 800 nM (P_o 0.14). Figure 4B shows that the closed times seen in the presence of NxTX−IbTX II are distinct from those seen in the control. Figure 4C shows that these dose-dependent effects of NxTX−IbTX II on P_o are well described by a single-site binding isotherm with a K_d value of 222 nM. This value is more than 50-fold tighter than the value measured under high external ionic strength conditions (i.e., 150 mM KCl outside and 10 mM KCl inside). Moreover, we observe a similar increase in affinity at low external ionic strength for all of the NxTX−IbTX chimera; see Tables 3 and 4. Thus, these low external ionic strength conditions, with 30 mM KCl outside and 150 mM KCl inside, promote a high-affinity interaction between the NxTX−IbTX chimera and the maxi-K channel. The high-affinity interaction observed at low external ionic strength also allows us to more readily quantify the interaction of these chimeras with the maxi-K channel.

NxTX−IbTX Mutants Inhibit the Maxi-K Channel with Rapid Blocking Kinetics. To measure the chimera blocking rates, we employed the method of amplitude distribution analysis (*24, 25*). This approach was necessary because under many conditions the NxTX−IbTX block times are not well separated from maxi-K channel gating kinetics. In addition, under low ionic strength conditions the NxTX−IbTX-II unblocked times approach the filtered dead time of the bilayer system. Thus, under these conditions the short unblock periods are not detected. The net effect of this is to yield apparently slower k_{on} values and apparently slower k_{off} values;

see Figure 4C. Thus, amplitude distribution analysis considerably extends the kinetic range of measurable toxin blocking rates. The principle of this method is that the rates of toxin unblock and block can be obtained by fitting amplitude distributions from single, open channel current records to a theoretical β function; see Materials and Methods (*24, 25*).

The method of amplitude distribution requires that the effective filtered time constant exceed the sum of the time constants for block and unblock. Since the NxTX−IbTX chimera displays block times (T_{block}) on the order of 10−20 ms, the single-channel records must be highly filtered for this analysis, <20 Hz. Figure 5A shows the amplitude histograms from single maxi-K channel records in the presence of NxTX−IbTX II from Figure 4A that have been refiltered. The closed and open current levels are normalized to 0 and 1, respectively. As expected, the mean single-channel current amplitude decreases with increasing toxin concentrations. Moreover, these amplitude distributions are well described by the best fit to a β function (solid line). This suggests that a two-state process can describe NxTX−IbTX block of the maxi-K channel.

Figure 5C shows that the NxTX−IbTX II blocking rates are consistent with a two-state, pseudo-first-order binding reaction where pseudo-first-order association rate constants (filled circles), obtained from the fits in (A), increase linearly with toxin concentration. The k_{on} value obtained from the slope of this line was 2.6×10^8 M^{-1} s^{-1}. In contrast, the blocking rates (filled squares) do not change with concentra-

tion and describe a k_{off} value of 55 s^{-1} (T_{block} = 18 ms). This T_{block} value is similar to the mean closed time observed from a closed time distribution when toxin inhibition is ~85%; see Figure 4B. Moreover, the K_d value of 245 nM obtained from k_{off}/k_{on} is nearly identical to values we obtain from dose-dependent effects of either P_o (Figure 4C) or relative current amplitude (Figure 5B). At low toxin concentrations, the association and dissociation rates obtained from blocked and unblocked distributions (open symbols) closely agreed with those obtained from amplitude distribution analysis (closed symbols). However, at higher toxin concentrations toxin unblocked times approached the dead time of the system, yielding apparently slower association and dissociation rates. Thus, compared to the dwell-time analysis, the amplitude distribution analysis provides a robust measure of blocking rates for the NxTX−IbTX chimera. Moreover, the NxTX−IbTX II association rate measured with low external ionic strength, $(1.8 \pm 0.8) \times 10^8$ M^{-1} s^{-1}, is ~100-fold faster than the association rate measured with high external ionic strength, $(2.2 \pm 1) \times 10^6$ M^{-1} s^{-1}; see Tables 3 and 4. Thus, low external ionic strength conditions promote a high-affinity NxTX−IbTX interaction with the maxi-K channel that results from fast association rates. The NxTX−IbTX chimera T_{block}, which are inversely related to the dissociation rates, are short, ranging from 5 to 20 ms for the four different chimeras; see Table 4. Thus, the NxTX−IbTX chimeras also display rapid dissociation kinetics. These blocked times are >3000-fold faster than those observed for other high-affinity blockers of the maxi-K channel (*1, 31*) and suggest that interactions at the NxTX−IbTX binding surface are not optimal.

NxTX−IbTX Chimera Show Dramatic Differences in Their Interaction with Kv1.3 vs Maxi-K Channel Outer Vestibules. The NxTX−IbTX chimeras are NxTX mutants that differ in the length of their α-carbon backbone and in critical maxi-K channel contact residues; see Figure 1. To understand how these features contribute to specificity for the Kv1.3 over maxi-K channels, we also examined their interaction with the Kv1.3 channel. The NxTX−IbTX I mutant contains six residues from the α/β turn in IbTX; see Table 1. Compared to NxTX, NxTX−IbTX I displays a 50-fold weaker affinity for the Kv1.3 channel; see Table 2. In contrast, this same mutation causes a tighter interaction with the maxi-K channel compared to wild type; see Table 3. This suggests that residues in the α/β turn of the α-KTx structure are important determinants of toxin binding specificity.

The remaining three chimeras, NxTX−IbTX II, NxTX−IbTX III, and NxTX−IbTX IV, also display striking differences in their interactions with maxi-K and Kv1.3 channels. To more easily compare the different effects of these chimeras, Figure 6 describes changes in binding free energy relative to NxTX−IbTX I for the Kv1.3 (hatched bars) and maxi-K (open bars) channels. The cartoon of the chimera sequences, in the figure, shows relative changes in the length of the α-carbon backbone and in critical contact residues. The NxTX−IbTX II, NxTX−IbTX III, and NxTX−IbTX IV all differ from NxTX−IbTX I in deletion of the C-terminal residue. These three mutants show a 4−40-fold tighter interaction with the maxi-K channel. Interestingly, this increase in affinity is derived primarily from an increase in the toxin k_{on} value (Table 4).
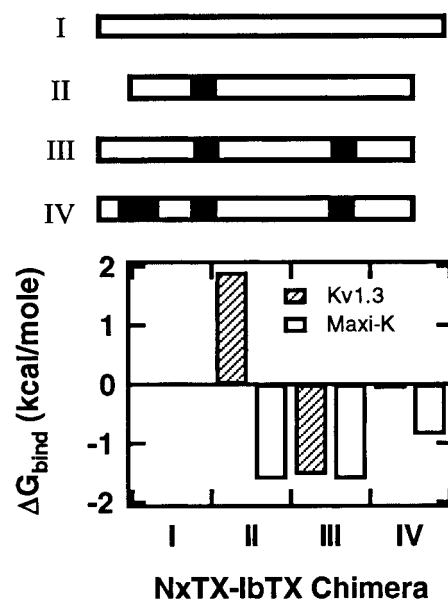

FIGURE 6: Effects of NxTX−IbTX mutations on binding free energy profiles for the Kv1.3 and maxi-K channels. Changes in binding free energy (ΔG_{bind}) for NxTX−IbTX II, NxTX−IbTX III, and NxTX−IbTX IV relative to NxTX−IbTX I for the Kv1.3 (hatched bars) and maxi-K channel (open bars) are calculated from K_d values in Tables 2 and 4, respectively. $\Delta G_{bind} = -RT \ln(K_{d(mt)}/K_{d(wt)})$, where $K_{d(wt)}$ describes K_d values for NxTX−IbTX I and $K_{d(mt)}$ describes K_d values for either NxTX−IbTX II, NxTX−IbTX III, or NxTX−IbTX IV. The cartoon of the NxTX−IbTX linear amino acid sequence shows changes in the relative length of the chimera and relative locations of site-directed mutations. See Table 1 of amino acid sequences for details.

In contrast, the chimeras display a completely different pattern of interaction with the Kv1.3 channel. For instance, NxTX−IbTX II displays a >30-fold weaker interaction relative to NxTX−IbTX I. NxTX−IbTX II is the shortest chimera, 36 amino acids, with a deletion of the N- and C-terminal residues relative to NxTX−IbTX I. Surprisingly, reinsertion of the N-terminal Thr, NxTX−IbTX III, dramatically increases the affinity for the Kv1.3 channel >300-fold, corresponding to a change in binding free energy of 3.4 kcal/mol. The importance of this N-terminal region to Kv1.3 binding is also illustrated by the fact that the I2F/I3D mutation of NxTX−IbTX III, NxTX−IbTX IV, causes an ~20-fold weakening of binding to the Kv1.3 channel. In contrast, these same mutations cause only modest changes in binding free energy for the maxi-K channel. These findings suggest that the N-terminal region of NxTX is critical to Kv1.3 binding and thus may be an important determinant of binding specificity.

DISCUSSION

Characteristics of the Kv1.3 NxTX Binding Surface. In this work we wanted to explore whether the specificity of the α-KTx peptides for different K channels is controlled by specific toxin residues or by more general features of the toxin α-carbon backbone. To delineate these effects, we generated NxTX mutants in which either site-specific residues or features of the α-carbon backbone were altered. As a model for K channel specificity, we examined the interaction of these NxTX mutants with two K channels that display remarkably different patterns of specificity for the different subfamilies of α-KTx peptides. The maxi-K channel

displays an extraordinary degree of specificity for peptides from the α-KTx 1.x subfamily. All of these peptides interact with the maxi-K channel with high affinity, in the low nanomolar range (*12*). In contrast, peptides from the α-KTx 3.x subfamilies display >1000-fold weaker interaction (*12*), while peptides from the α-KTX 2.x display no measurable interaction with the maxi-K channel (*19*). Indeed, in this work we estimate that the NxTX K_d value for the maxi-K channel exceeds 1 mM. In striking contrast, the Kv1.3 channel is among the most promiscuous of Kv channels in that it displays high-affinity interactions with peptides from all three of the α-KTx subfamilies (*16*). These remarkable differences in α-KTx specificity present the uncommon opportunity to explore fundamental differences in the architectures of the maxi-K and Kv channel vestibules.

The interactions of site-directed NxTX mutants with the Kv1.3 channel help to define the NxTX binding surface. In this work, we showed that mutations of residues protruding from the NxTX β-sheet face and in the α/β turn cause large changes in binding free energy relative to wild type. Thus, the β-sheet face and α/β turn in NxTX form part of its interaction surface with the Kv1.3 channel. This finding is consistent with studies on other α-KTx peptides and Kv channels which showed that residues comprising the β-sheet face and in the α/β turn form the toxin binding surface (*6, 8−10*). Thus, through site-directed mutagenesis our work supports that, similar to other α-KTx peptides, the β-sheet face in NxTX forms its binding surface with the Kv1.3 channel.

A surprising finding from this work is that the N-terminal region of NxTX is critical to its interaction with the Kv1.3 channel. This is based on the finding that NxTX−IbTX III displays >300-fold tighter interaction with the Kv1.3 channel relative to NxTX−IbTX II (Figure 6). Thus, reinsertion of the N-terminal Thr in NxTX produces a 300-fold tighter affinity for the Kv1.3 channel. How can reinsertion of this N-terminal Thr cause such a large increase in affinity? One possible explanation is that the cationic N-terminal ammonium groups in these two chimeras may be interacting with different microscopic environments that differ in their ability to solvate a positive charge. Previous studies on a ChTX-sensitive Shaker Kv channel mutant showed that the ionization state of the N-terminus in ChTX (α-KTx 1.1) has a profound effect on toxin binding free energy (*8*). These same studies showed that mutating successive residues from the N-terminus (residues 2−6) exerted relatively small effects on toxin binding free energy. Thus, these residues are not critical to binding. Together, our studies with the NxTX−IbTX mutants and studies of ChTX block of Shaker can also explain the seemingly contradictory finding that deletion of six residues from ChTX, ChTX-7−37, causes no change in its binding interaction with Kv1 channels (*31*). In this mutant, the cationic N-terminus of ChTX-7−37 is in a region not predicted to be part of the toxin binding surface. Collectively, our work and the work of others suggest that the α-KTx N-terminus comprises an important region of the toxin−Kv channel binding surface. While we cannot rule out the role of other noncovalent interactions, together these findings also suggest that the α-KTx N-terminus may be an important sensor of the electrostatic environment of the channel vestibule.

Characteristics of the Maxi-K Channel NxTX−IbTX Binding Interaction. In this work we have shown that the maxi-K channel displays an extraordinary ability to discriminate against NxTX with an estimated K_d value exceeding 1 mM. Compared to other members of the α-KTx 1.x subfamily (IbTX and ChTX), this represents more than a millionfold difference in binding affinity (*31*). By changing the NxTX α-carbon backbone, we generated NxTX−IbTX mutants which are capable of inhibiting current through maxi-K channels with high nanomolar to micromolar affinity, under low and high external ionic strength conditions, respectively. Evidence that these NxTX−IbTX chimeras occlude the pore of the maxi-K channel comes from the finding that the toxin-blocked times decrease ∼3-fold when the membrane potential is depolarized from −20 to +30 mV;, see Table 4. This effect is similar to effects observed for ChTX (*2*) and IbTX (*23*) block of the maxi-K channel. Moreover, this finding is consistent with a well-founded model where the stability of the α-KTx channel complex is regulated by the equilibrium occupancy of a voltage-dependent K^+ binding site in the channel pore (*1, 2, 23, 32*). In addition, we found that NxTX−IbTX II competes with an IbTX mutant in blocking current through the maxi-K channel (not shown). Thus, through these changes in the α-carbon backbone we were able to generate NxTX mutants that bind to and occlude the pore of the maxi-K channel.

The maxi-K channel from smooth muscle exceptionally discriminates against NxTX. This finding was surprising given previous studies showing that native NxTX blocked a skeletal muscle maxi-K channel with high nanomolar affinity, K_d 450 nM (*33*). The maxi-K channel from bovine aortic smooth muscle consists of pore-forming α and regulatory β1 subunit in a 1:1 stoichiometry (*34*). In contrast, we have recently shown that maxi-K channel complexes from skeletal muscle are not functionally associated with β1 subunits (*35*). Moreover, ChTX block of the maxi-K channel is sensitive to β1 subunit expression (*35*). Thus, it is possible that the presence of the β1 subunit in smooth muscle maxi-K channels prevents a high-affinity interaction with NxTX. However, we found that neither synthetic nor recombinant NxTX blocks maxi-K channels from rabbit skeletal muscle (not shown). Thus, β1 subunit expression may not influence NxTX block of the maxi-K channel. An alternative explanation for the discrepancy is that native NxTX is amidated at the C-terminus (*36*) while recombinant and synthetic NxTX are not. Amidation of the C-terminal residue removes a negative charge from the toxin binding surface that may help to promote a tighter binding interaction with the maxi-K channel.

A general finding for the four NxTX−IbTX mutants is that their affinities for the maxi-K channel span a small range compared to the Kv1.3, 10-fold vs 500-fold. The small range in binding free energies is expected from a weak, binding interaction. If the overall binding free energy is small, then by definition each microscopic interaction contributes a comparatively small amount to the total binding free energy. Consistent with this weak toxin−channel interaction, we found that the kinetics of block for all of the NxTX−IbTX mutants are rapid, ranging from 5 to 40 ms. These blocked times are ∼10 000-fold faster than either ChTX or IbTX blocked times (*31*). Thus, the NxTX−IbTX−maxi-K channel interaction surface may not contain an optimal set of

microscopic interactions. The solution ^{1}H NMR structures of NxTX−IbTX I and NxTX−IbTX II, in a companion paper, provide possible structural explanations for the relatively unstable toxin channel complexes (*37*).

The Role of the α-Carbon Backbone in Defining Specificity. A critical finding of this work is that the α-carbon backbone is an important determinant of α-KTx binding specificity. A distinctive feature of the α-KTx 1.x subfamily of peptides is the short length of its α-carbon backbone, 37 amino acids. The backbone length for the α-KTx 2.x and α-KTX 3.x subfamilies are longer by one or two amino acids. In NxTX (α-KTx 2.1), the two extra residues extend the N- and C-termini relative to the α-KTx 1.x subfamily (*12, 22, 28*). Consequently, these extra residues increase the length of the first and third antiparallel β-strands of the β-sheet face in NxTX; see Figure 1 (*12*). Thus, the β-sheet face in NxTX is increased in length relative to that of the α-KTx 1.x peptide toxins. The α-KTx 2.x and α-KTx 1.x subfamilies also differ in their α/β turns (*12*). The NxTX−IbTX chimeras were designed to understand how these differences in the α-carbon backbone influence specificity for the Kv and maxi-K channels.

To test the role of the α/β turn in defining α-KTx specificity, we generated a NxTX mutant, NxTX−IbTX I, which contains residues from the α/β turn in IbTX (Table 1). This mutation caused a 50-fold weaker interaction with the Kv1.3 channel and a tighter interaction with the maxi-K channel, respectively. To obtain a better estimate of the increase in NxTX−IbTX I affinity for the maxi-K channel compared to NxTX, we examined the inhibition of monoiodinated IbTX-D19Y/Y36F binding to bovine aortic sarcolemmal membranes as described (*15*). This assay revealed that specific NxTX−IbTX I binding to maxi-K channel complexes is >150-fold tighter than NxTX (not shown). The data presented in this work do not allow us to ascertain whether these effects on the maxi-K and Kv1.3 channels result from subtle changes in the toxin backbone fold or from the identity of specific residues in this turn. However, the observed functional effects clearly illustrate that the α/β turn in the α-KTx peptides plays an important role in defining specificity.

The length of the α-carbon backbone may also be an important factor in specificity. The extra length of the NxTX backbone appears to prevent its binding to the maxi-K channel. This is supported by the finding that all of the chimera block the maxi-K channel with measurable affinity, and all of these mutants are decreased in the length of their α-carbon backbone compared to NxTX; see Table 1. Evidence that the length at the C-terminus prevents NxTX binding to the maxi-K channel comes from the finding that NxTX−IbTX II and NxTX−IbTX III block the maxi-K channel with 15-fold tighter affinity that NxTX−IbTX I; see Figure 6. In contrast, the Kv1.3 channel does not discriminate among the α-KTx peptides that differ in length (*16*). From solution structures for NxTX−IbTX I and NxTX−IbTX II it is clear that deletion of the C-terminal residue in NxTX−IbTX II results in a β-sheet that is reduced in length (*37*). Together, these results suggest that the maxi-K channel vestibule is more sensitive to the dimensions of the toxin β-sheet than is the Kv1.3 channel.

In this work, we clearly showed that specific α-KTx residues are not the only determinants of specificity for Kv vs maxi-K channels. Moreover, our data support the fact that the α-KTx α-carbon backbone plays an important role in defining its molecular discrimination of the two families of K channels. The NxTX−IbTX chimeras we generated were altered in the α/β turn and in backbone length compared to NxTX. However, the data presented cannot distinguish between specific residue interactions, changes in backbone fold, or changes in the toxin β-sheet. In a companion paper (*37*), the solution ^{1}H NMR structures of NxTX−IbTX I and NxTX−IbTX II suggest that the extra length of the toxin β-sheet face may be an important feature for molecular discrimination between maxi-K and Kv1.3 channels. However, other features of the NxTX may also contribute to this molecular discrimination. All of the NxTX−IbTX mutants showed increased affinity for the maxi-K channel compared to NxTX. However, this interaction of the tightest binding chimera (NxTX−IbTX III) was >1000-fold weaker compared to IbTX (Table 4). This relatively weak affinity may arise from changes in the backbone fold that introduce unfavorable interactions with the channel. Alternatively, other features of the NxTX structure may contribute to its weak interaction. For instance, superposition of IbTX and NxTX also reveals differences in the helix turn. This helix turn also forms a critical part of the toxin binding surface in maxi-K (*11*) and the Shaker Kv channel (*8, 38*). In particular, ChTX block of the Shaker Kv channel is especially sensitive to the size of toxin residues in this helix turn and to the size of interacting residues in Shaker (*38*). Because the toxin helix turn also forms the maxi-K channel binding surface, some of the molecular discrimination against NxTX may arise from unfavorable interactions at this interface. A further test of the role of the α-carbon backbone in specificity would be to identify maxi-K channel residues that relieve these apparent steric constraints and allow a high-affinity interaction between NxTX and the maxi-K channel.

Previous studies of toxin binding and specificity only narrowly considered the role of specific residues in defining specificity. The approach in this work of altering the α-KTx α-carbon backbone expands our understanding of molecular discrimination among K channels, and it provides an important means for identifying fundamental differences in the architectures of the Kv and maxi-K channel vestibules.

REFERENCES

1. Giangiacomo, K. M., Garcia, M. L., and McManus, O. B. (1992) *Biochemistry 31*, 6719−6727.
2. MacKinnon, R., and Miller, C. (1988) *J. Gen. Physiol. 91*, 335−349.
3. Goldstein, S. A., and Miller, C. (1993) *Biophys. J. 65*, 1613−1619.
4. MacKinnon, R., and Miller, C. (1989) *Science 245*, 1382−1385.
5. MacKinnon, R., Heginbotham, L., and Abramson, T. (1990) *Neuron 5*, 767−771.

6. Aiyar, J., Withka, J. M., Rizzi, J. P., Singleton, D. H., Andrews, G. C., Lin, W., Boyd, J., Hanson, D. C., Simon, M., Dethlefs, B., et al. (1995) *Neuron 15*, 1169−1181.

7. Aiyar, J., Rizzi, J. P., Gutman, G. A., and Chandy, K. G. (1996) *J. Biol. Chem. 271*, 31013−31016.

8. Goldstein, S. A., Pheasant, D. J., and Miller, C. (1994) *Neuron 12*, 1377−1388.

9. Hidalgo, P., and MacKinnon, R. (1995) *Science 268*, 307−310.

10. Ranganathan, R., Lewis, J. H., and MacKinnon, R. (1996) *Neuron 16*, 131−139.

11. Stampe, P., Kolmakova-Partensky, L., and Miller, C. (1994) *Biochemistry 33*, 443−450.

12. Giangiacomo, K. M., Gabriel, J., Fremont, V., and Mullmann, T. J. (1999) *Perspect. Drug Discovery Des. 15/16*, 167−186.

13. Miller, C. (1995) *Neuron 15*, 5−10.

14. Galvez, A., Gimenez-Gallego, G., Reuben, J. P., Roy-Contancin, L., Feigenbaum, P., Kaczorowski, G. J., and Garcia, M. L. (1990) *J. Biol. Chem. 265*, 11083−11090.

15. Koschak, A., Koch, R. O., Liu, J., Kaczorowski, G. J., Reinhart, P. H., Garcia, M. L., and Knaus, H. G. (1997) *Biochemistry 36*, 1943−1952.

16. Grissmer, S., Nguyen, A. N., Aiyar, J., Hanson, D. C., Mather, R. J., Gutman, G. A., Karmilowicz, M. J., Auperin, D. D., and Chandy, K. G. (1994) *Mol. Pharmacol. 45*, 1227−1234.

17. Escobar, L., Root, M. J., and MacKinnon, R. (1993) *Biochemistry 32*, 6982−6987.

18. Slaughter, R. S., Shevell, J. L., Felix, J. P., Garcia, M. L., and Kaczorowski, G. J. (1989) *Biochemistry 28*, 3995−4002.

19. Garcia-Calvo, M., Leonard, R. J., Novick, J., Stevens, S. P., Schmalhofer, W., Kaczorowski, G. J., and Garcia, M. L. (1993) *J. Biol. Chem. 268*, 18866−18874.

20. Sanger, F., Nicklen, S., and Coulson, A. R. (1977) *Proc. Natl. Acad. Sci. U.S.A. 74*, 5463−5467.

21. Naini, A. A., Shimony, E., Kozlowski, E., Shaikh, T., Dang, W., and Miller, C. (1996) *Neuropharmacology 35*, 915−921.

22. Johnson, B. A., Stevens, S. P., and Williamson, J. M. (1994) *Biochemistry 33*, 15061−15070.

23. Mullmann, T. J., Munujos, P., Garcia, M. L., and Giangiacomo, K. M. (1999) *Biochemistry 38*, 2395−2402.

24. Yellen, G. (1984) *J. Gen. Physiol. 84*, 157−186.

25. Yellen, G. (1984) *J. Gen. Physiol. 84*, 187−199.

26. Hamill, O. P., Marty, A., Neher, E., Sakmann, B., and Sigworth, F. J. (1981) *Pfluegers Arch. 391*, 85−100.

27. Christian, E. P., Spence, K. T., Togo, J. A., Dargis, P. G., and Patel, J. (1996) *J. Membr. Biol. 150*, 63−71.

28. Dauplais, M., Gilquin, B., Possani, L. D., Gurrola-Briones, G., Roumestand, C., and Menez, A. (1995) *Biochemistry 34*, 16563−16573.

29. MacKinnon, R., LaTorre, R., and Miller, C. (1989) *Biochemistry 28*, 8092−8099.

30. Anderson, C. S., MacKinnon, R., Smith, C., and Miller, C. (1988) *J. Gen. Physiol. 91*, 317−333.

31. Giangiacomo, K. M., Sugg, E. E., Garcia-Calvo, M., Leonard, R. J., McManus, O. B., Kaczorowski, G. J., and Garcia, M. L. (1993) *Biochemistry 32*, 2363−2370.

32. Park, C. S., and Miller, C. (1992) *Neuron 9*, 307−313.

33. Valdivia, H. H., Smith, J. S., Martin, B. M., Coronado, R., and Possani, L. D. (1988) *FEBS Lett. 226*, 280−284.

34. Giangiacomo, K. M., Garcia-Calvo, M., Knaus, H. G., Mullmann, T. J., Garcia, M. L., and McManus, O. (1995) *Biochemistry 34*, 15849−15862.

35. Giangiacomo, K. M., Fremont, V., Mullmann, T. J., Hanner, M., Cox, R. H., and Garcia, M. L. (2000) *Biochemistry 39*, 6115−6122.

36. Garcia, M. L., Hanner, M., Knaus, H. G., Koch, R., Schmalhofer, W., Slaughter, R. S., and Kaczorowski, G. J. (1997) *Adv. Pharmacol. 39*, 425−471.

37. Ferrat, G., Bernard, C., Fremont, V., Mullmann, T. J., Giangiacomo, K. M., and Darbon, H. (2001) *Biochemistry 40*, 10998−11006.

38. Goldstein, S. A., and Miller, C. (1992) *Biophys. J. 62*, 5−7.

39. Johnson, B. A., and Sugg, E. E. (1992) *Biochemistry 31*, 8151−8159.